ACS Infectious Diseases

pubs.acs.org/journal/aidcbc

Article

Targeting Polyamines Inhibits Coronavirus Infection by Reducing Cellular Attachment and Entry

Mason R. Firpo, Vincent Mastrodomenico, Grant M. Hawkins, Matthieu Prot, Laura Levillayer, Tom Gallagher, Etienne Simon-Loriere, and Bryan C. Mounce*

Cite This: https://dx.doi.org/10.1021/acsinfecdis.0c00491

Read Online

ACCESS | Metrics & More | Article Recommendations

ABSTRACT: Coronaviruses first garnered widespread attention in 2002 when the severe acute respiratory syndrome coronavirus (SARS-CoV) emerged from bats in China and rapidly spread in human populations. Since then, Middle East respiratory syndrome coronavirus (MERS-CoV) emerged and still actively infects humans. The recent SARS-CoV-2 outbreak and the resulting disease (coronavirus disease 2019, COVID19) have rapidly and catastrophically spread and highlighted significant limitations to our ability to control and treat infection. Thus, a basic understanding of entry and replication mechanisms of coronaviruses is necessary to rationally evaluate potential antivirals. Here, we show that polyamines, small metabolites synthesized in human cells, facilitate coronavirus replication and the depletion of polyamines with FDA-approved molecules significantly reduces coronavirus replication. We find that diverse coronaviruses, including endemic and epidemic coronaviruses, exhibit reduced attachment and entry into polyamine-depleted cells. We further demonstrate that several molecules targeting the polyamine biosynthetic pathway are antiviral *in vitro*. In sum, our data suggest that polyamines are critical to coronavirus replication and represent a highly promising drug target in the current and any future coronavirus outbreaks.

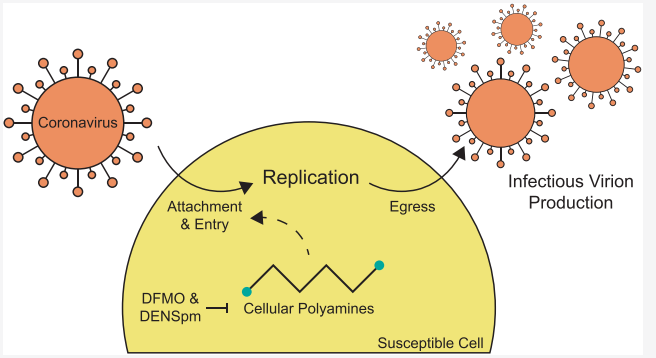

KEYWORDS: *coronavirus, polyamines, binding, SARS-CoV-2*

Coronaviruses are significant human pathogens with significant epidemic potential. Recurring coronavirus outbreaks wreak havoc on human health and activity, as demonstrated by the original severe acute respiratory syndrome coronavirus (SARS-CoV) outbreak of 2002, the Middle East respiratory syndrome coronavirus (MERS-CoV) of 2011 to present day,[1] and the newly emergent SARS-CoV-2 of 2019 to present.[2] Each of these viruses emerged from zoonotic sources and were rapidly transmitted through human populations, requiring urgent attention due to the number of infections, combined with mortality rates of up to 35% in the case of MERS-CoV.[3] In addition to their epidemic potential, coronaviruses are common human pathogens, with several endemic coronaviruses causing recurrent infections with generally mild symptoms.[4,5] Treatments for SARS-CoV-2, as well as other coronaviruses, include remdesivir, a base analog that exhibited promising clinical efficacy.[6,7] A dearth of additional antivirals is available to treat or prevent infections. The omnipresence, unpredictable epidemic potential, and significant impact on human health make the investigation into potential antiviral compounds essential to battle current and future coronavirus outbreaks.

Polyamines are small aliphatic metabolites synthesized by mammalian cells to support cellular processes such as cell cycling, transcription, and translation.[8−10] The polyamines putrescine, spermidine, and spermine (Figure 1A) are synthesized from an ornithine precursor through the enzyme ODC1. Several specific and potent inhibitors of the polyamine biosynthetic pathway have been developed and are FDA approved. The ODC1 inhibitor difluoromethylornithine (DFMO) is approved for the treatment of trypanosomiasis.[11] In fact, DFMO exhibits low toxicity and mild side effects.[12] Topical DFMO has also been developed and is sold as Vaniqa to reduce hair growth.[13] Viruses rely on polyamines for varied stages in replication, including polymerase activity,[14] cell binding,[15] and viral protein translation.[15,16] Polyamine depletion via DFMO effectively reduces the replication of

Special Issue: Antiviral Therapeutics

Received: July 10, 2020
Published: September 23, 2020

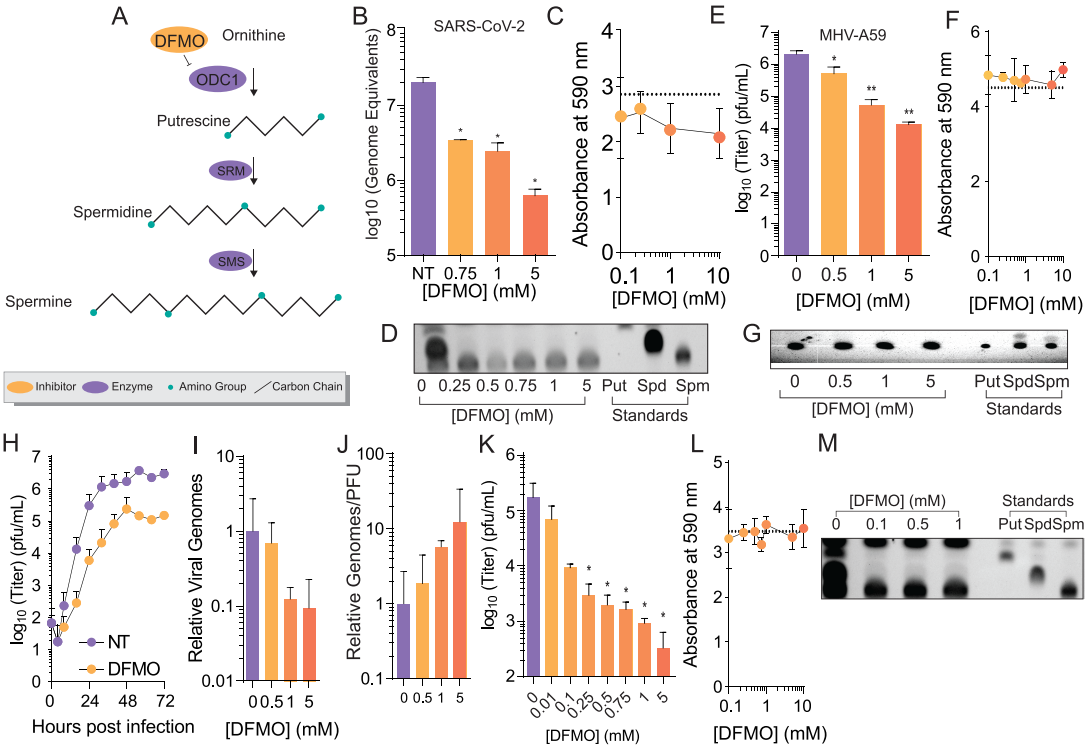

Figure 1. Polyamine synthesis inhibitor DFMO limits coronavirus replication. (A) Schematic of the polyamine pathway. The polyamines putrescine, spermidine, and spermine are synthesized from ornithine via ornithine decarboxylase (ODC1), which is inhibited by difluoromethylornithine (DFMO). (B) Vero-E6 cells treated with increasing doses of DFMO were infected with SARS-CoV-2 at an MOI of 0.1 for 24 h, and viral genomes were measured and converted to titer equivalents via a standard curve. (C) Vero-E6 cells were treated with escalating DFMO doses and viability and (D) polyamine levels were measured. (E) BHK-R cells were treated with DFMO as indicated and infected with MHV at an MOI of 0.01 for 48 h. (F) Cellular viability levels were measured and (G) polyamine depletion was confirmed by chromatography. (H) BHK-R cells were treated with 1 mM DFMO and infected with MHV at an MOI of 0.01. Viral titers were determined after several rounds of replication. (I) MHV genomes from samples in (E) were quantified by qRT-PCR and compared to viral titers to quantify the relative number of genomes to PFU (J). (K) HeLa-R cells were treated with escalating doses of DFMO and infected with MHV at an MOI of 0.01 for 48 h. (L) HeLa-R cells exposed to DFMO for 4 days were analyzed for viability. (M) Depletion of polyamines was confirmed by chromatography. *$p < 0.05$, **$p < 0.01$, and ***$p < 0.001$ by the Student's t test. Data from at least three independent experiments.

diverse viruses *in vitro* and *in vivo* with minimal cytotoxicity.[17,18] Prior work demonstrated that MERS-CoV was sensitive to the polyamine inhibitor DFMO *in vitro* at a dose of 500 μM,[19] suggesting that polyamines function in coronavirus replication. Whether and how polyamines function in the replication of other coronaviruses remain to be investigated.

The study of human epidemic coronaviruses is limited due to requisite biosafety protocols. Thus, murine model systems have been developed to study coronavirus replication and pathogenesis with significantly reduced risk. Murine hepatitis virus (MHV) is a common model system for coronavirus infection. MHV, a β-coronavirus, is related to the human epidemic coronaviruses, though it is safe to work with in the laboratory. The MHV model is well characterized,[20,21] and combined with its ease of use, it provides a significant opportunity to study coronavirus infection.

Using the MHV model system, we investigated a role for polyamines in coronavirus infection. We observe that polyamine depletion via DFMO limits virus replication and that polyamines support virus infection at the stage of attachment: polyamine depletion reduces virus binding to susceptible cells. We extend this phenotype to the human endemic coronavirus NL63 as well as the pandemic SARS-CoV-2. Additionally, we demonstrate that several molecules targeting the polyamine pathway, including FDA-approved pharmaceuticals, exhibit significant antiviral activity. Together, our data highlight a role for polyamines in coronavirus replication and suggest that targeting polyamines may be a viable preventative or treatment option for coronavirus infection.

RESULTS

Polyamine Depletion Limits Coronavirus Replication.

To determine if coronaviruses are susceptible to polyamine depletion, we treated Vero-E6 cells with doses of DFMO ranging from 750 μM to 5 mM for 4 days prior to infection with SARS-CoV-2 at a multiplicity of infection (MOI) of 0.1 plaque forming units (pfu) per cell. Released viral genomes were then measured at 24 h post-infection (hpi) and converted to virus equivalents using a standard curve comparing known infectious titers and genomes. We observed that DFMO significantly reduced SARS-CoV-2 genomes, greater than 50-fold at 5 mM, with an IC50 (50% inhibitory concentration) value of 230 μM (Figure 1B). To confirm that DFMO was not cytotoxic, we measured the viability of Vero-E6 cells treated with escalating doses of DFMO and calculated a CC50 (50% cytotoxic concentration) value of 11 mM (Figure 1C; summarized in Table 1). We further confirmed that DFMO treatment at these concentrations successfully depleted polyamines via thin layer chromatography (TLC; Figure 1D).

To expand on this work, we turned to the MHV model system. As with our experiments with SARS-CoV-2, BHK-21

https://dx.doi.org/10.1021/acsinfecdis.0c00491
ACS Infect. Dis. XXXX, XXX, XXX−XXX

Table 1. Properties of the Compounds Used in These Studies

inhibitor	virus	cells	IC50 (μM)	CC50 (mM)	SI
DFMO	MHV-A59	BHK-R	380	3.8	10
		HeLa-R	7.0	16	2300
DENSpm		HeLa-R	1.6	35	7100
CPX		BHK-R	2.2	76	35000
DEF		BHK-R	54	60	1100
GC7		BHK-R	7.4	42	5600
DFMO	SARS-CoV-2	Vero-E6	230	11	48

cells expressing the MHV receptor (BHK-R)[22] were pretreated with various concentrations of DFMO 4 days before infection with an MOI of 0.01. Supernatant was collected 48 h post-infection (hpi), and titers were measured with a plaque assay on BHK-Rs. Viral titers were significantly reduced in a dose-dependent manner, with an IC50 value of 380 μM (Figure 1E). We confirmed that DFMO depleted polyamines in these cells by TLC (Figure 1G), especially levels of putrescine and spermidine, as previously described.[14] To test if DFMO remained antiviral over multiple rounds of infection, BHK-Rs were treated with DFMO and infected at an MOI of 0.01. Supernatant was collected and titered at the indicated time points (Figure 1H). DFMO reduced viral titers compared to the no treatment group up to 72 h, and viral titers in DFMO-treated cells plateaued at a lower level than untreated controls, suggesting that MHV was unable to overcome polyamine depletion over several rounds of replication. We observed that DFMO had modest toxicity in BHK-R cells with a CC50 of 3.8 mM (Figure 1F), giving a selectivity index (SI) of 10. Finally, we measured the relative number of genomes present in the supernatant from the infected cells. Following treatment and infection, we purified, reverse-transcribed, and measured viral genomes by qPCR using specific primers and observed reduced genome levels with DFMO treatment (Figure 1I). Using the data from infectious titers (Figure 1E) and viral genomes (Figure 1I), we calculated the specific infectivity (genomes per PFU) and observed that DFMO treatment increased the ratio of genomes to titer (Figure 1J), similar to previous findings with bunyaviruses and polyamine depletion.[23] Thus, polyamines enhance coronavirus infection and maintain a specific infectivity of MHV.

To address the role of cell type, we tested the ability of DFMO to restrict virus replication in HeLa cells expressing the MHV receptor (HeLa-R). Cells were pretreated with DFMO and infected at an MOI of 0.01 for 48 h. We observed a decline in virus replication, more pronounced than on BHK-R cells, with an IC50 value of approximately 7.0 μM (Figure 1K). We confirmed that DFMO treatment of HeLa-R cells reduced polyamines (Figure 1M) and verified that DFMO was not toxic to these cells (Figure 1L). The CC50 of DFMO in HeLa cells was 16 mM, and thus, the selectivity index was 2300.

Polyamines Facilitate Coronavirus Replication. DFMO restricts virus replication by reducing cellular polyamine pools.[19] However, excess polyamines do not enhance virus replication, according to work based on chikungunya virus.[14] Recent work has suggested that polyamines may serve coronavirus replication.[24] To determine if exogenously supplied polyamines serve an antiviral role, we treated BHK-R cells with increasing doses of the individual polyamines putrescine, spermidine, and spermine, from 1 to 100 μM. We measured cellular viability (Figure 2A) and infected these cells to measure viral titers at 48 hpi (Figure 2B). We observed that the polyamines significantly reduced cellular viability at approximately 5 μM, reflecting prior descriptions of high polyamine concentrations leading to apoptosis.[25,26] Despite this reduction in viability, we observed modestly reduced viral titers (Figure 2B). We measured polyamines in supplemented cells and observed that supplementation with any of the three polyamines resulted in only modest changes in cell-associated polyamines (Figure 2B, lower), as we previously described.[27] The reduced signal with high concentrations of spermidine and spermine likely was an artifact of reduced cellular viability at these doses.

To determine if DFMO-mediated virus restriction was a result of polyamine depletion, we treated BHK-R cells with

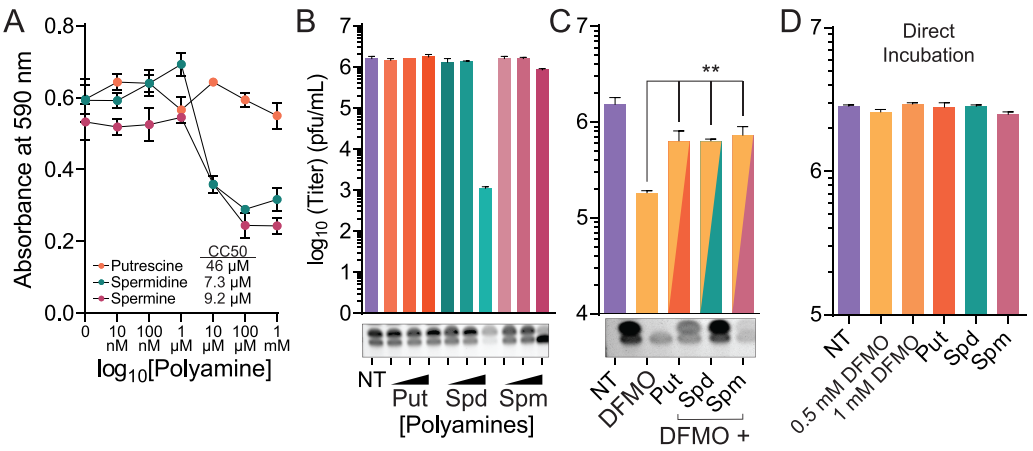

Figure 2. Polyamines facilitate coronavirus replication. (A) BHK-R cells were treated with escalating doses of putrescine, spermidine, and spermine, and cellular viability was measured 24 h later. Calculated CC50 values are in the inset. (B) BHK-R cells treated as in (A) were infected with MHV at an MOI of 0.01 and titered at 48 hpi (upper). Cell-associated polyamines were measured by chromatography (lower). (C) BHK-R cells were treated with 1 mM DFMO for 4 days prior to infection with MHV at an MOI of 0.01. At the time of infection, 1 μM polyamines were added to the cells. Viral titers were determined at 48 hpi (upper). Cell-associated polyamines were measured by chromatography (lower). (D) MHV was directly incubated with DFMO or 1 μM of the polyamines putrescine (put), spermidine (spd), and spermine (spm) for 24 h and then directly titered. **$p < 0.01$ by the Student's t test. Data from at least two independent experiments.

https://dx.doi.org/10.1021/acsinfecdis.0c00491
ACS Infect. Dis. XXXX, XXX, XXX−XXX

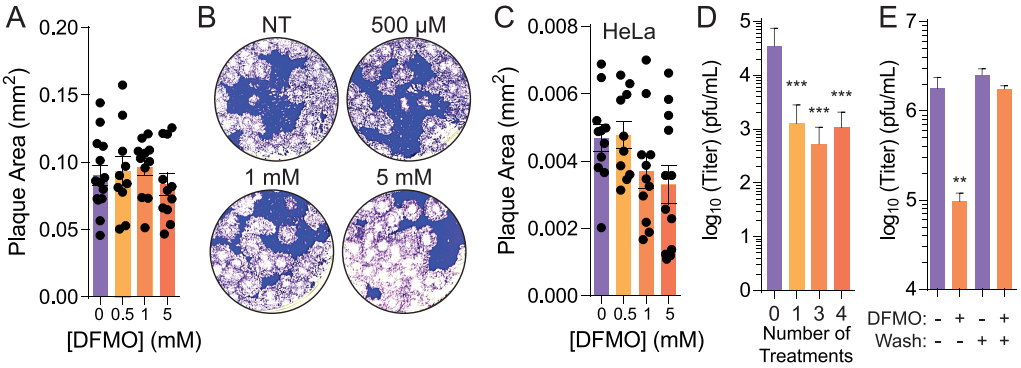

Figure 3. Polyamine depletion is antiviral prophylactically. Confluent monolayers of BHK-R cells were treated with DFMO at the time of infection with MHV and overlaid with agarose to form plaques. (A) Plaques were quantified 2 days later. (B) Representative plaques are shown from (A). (C) HeLa-R cells were infected and treated as in (A) and the plaque area was measured. (D) BHK-R cells were treated with 1.5 mM DFMO in one, three, or four doses prior to infection with MHV at an MOI of 0.01. Viral titers were determined by plaque assay at 48 hpi. (E) Cells were treated with 1 mM DFMO and then subsequently refed with fresh medium not containing DFMO 24 h before infection with MHV at an MOI of 0.01. Titers were determined at 24 hpi. $^{**}p < 0.01$ and $^{***}p < 0.001$ by the Student's t test. Representative data from at least three independent experiments. Individual plaque sizes are indicated in (A) and (C).

DFMO and, at the time of infection, supplemented with the individual polyamines putrescine, spermidine, and spermine at 1 μM, a level that did not affect cellular viability (Figure 2A). We observed that DFMO reduced viral titers and that supplementation with any of the individual polyamines rescued virus replication to untreated levels (Figure 2C). We confirmed the presence of these polyamines (Figure 2C, below) and observed that supplementation with any of the individual polyamines results in the accumulation of all three polyamines in the cells. To exclude the possibility that polyamines may directly inactivate viral particles, we directly incubated MHV with DFMO and each of the individual polyamines at 10 μM for 24 h and then titered the incubated virus. We observed that neither DFMO nor polyamines affected infectivity when incubated with virus, as titers were unchanged compared to untreated controls (Figure 2D). In sum, our data suggest that polyamines support virus yield and that supplementation of polyamines supports but does not enhance this yield and can instead be cytotoxic.

Polyamine Depletion Is Prophylactic. DFMO depletes polyamines by inhibiting ODC1, though time is required to deplete cellular polyamine pools and subsequently reduce viral titers.[14] Ideally, the treatment with antivirals commences after the initiation of infection, though identification of soon-to-be-infected individuals is impractical. Thus, to determine if we could treat cells with DFMO at the time of infection, which would be more clinically relevant, we determined whether DFMO suppresses plaque development when present in overlay media, as previously described.[19] We observed no changes in plaque size (Figure 3A) or morphology (Figure 3B) with DFMO supplementation to the media, suggesting that DFMO was not sufficiently antiviral when applied to cells after infection and highlighting that DFMO must be applied prophylactically to reduce coronavirus replication. We observed a small, though statistically insignificant change in HeLa-R cells (Figure 3C).

The use of DFMO as an anti-trypanosomal agent requires repeated dosing to reach a serum concentration high enough to inhibit trypanosome growth.[11,12,28] To mimic this, we treated BHK-R cells with 1.5 mM DFMO in a single treatment, three 500 μM treatments, or four 375 μM treatments equally spaced over the 4 days prior to infection. We observed that cells receiving multiple doses of the drug reduced cellular capacity to support virus production, similar to when the drug was delivered in a single dose (Figure 3D), suggesting that repeated dosing is as effective as a single drug treatment *in vitro*. Finally, we tested whether the antiviral effects of DFMO were reversed by removing the drug and replenishing cells with fresh media. We treated cells with 1 mM for 4 days and then removed and replaced the media with fresh media without drug for 24 h before infection. When we measured viral titers, we observed the DFMO treatment reduced infectious virus production, and this effect was completely reversed by replenishing the cells with fresh media, suggesting that DFMO's antiviral effect can be reversed by removing the drug.

Polyamines Facilitate Coronavirus Binding and Entry. We previously demonstrated that enteroviruses, flaviviruses, and bunyaviruses rely on polyamines for viral attachment and entry.[15] To test whether coronaviruses similarly rely on polyamines for attachment and entry, we performed a binding assay in cells treated with DFMO. We treated BHK-R cells with DFMO for 4 days prior to infection with 1000 pfu. After 5 min, unbound virus was washed away with PBS and cells were overlaid with agarose for a plaque assay, lacking DFMO in the overlay. Thus, DFMO is present only during binding of MHV to target cells and not for any other portion of the viral life cycle. Plaques were then allowed to form and were enumerated, representing bound and entered infectious virus. We observed that the attachment and plaque formation was significantly inhibited with DFMO treatment (Figure 4A, representative plaques for NT and 1 mM in Figure 4B). We expanded these results by infecting DFMO-treated BHK-R cells with MHV for 5 min, washing away unbound virus, and quantifying bound virus by qRT-PCR. We observed that, similar to our plaque formation assays, bound viral genomes were significantly reduced with DFMO treatment (Figure 4C). We confirmed that the cells expressed the MHV receptor (CECAM-1) by immunofluorescence (Figure 4D), regardless of DFMO treatment, suggesting that DFMO treatment was not directly reducing receptor availability. We recapitulated these results with HeLa-R cells and observed a similar reduction in virus binding with DFMO treatment (Figure 4E).

To expand to human coronaviruses, we tested HCoV-NL63 for binding to DFMO-treated Vero-E6 cells. Again, we

https://dx.doi.org/10.1021/acsinfecdis.0c00491
ACS Infect. Dis. XXXX, XXX, XXX−XXX

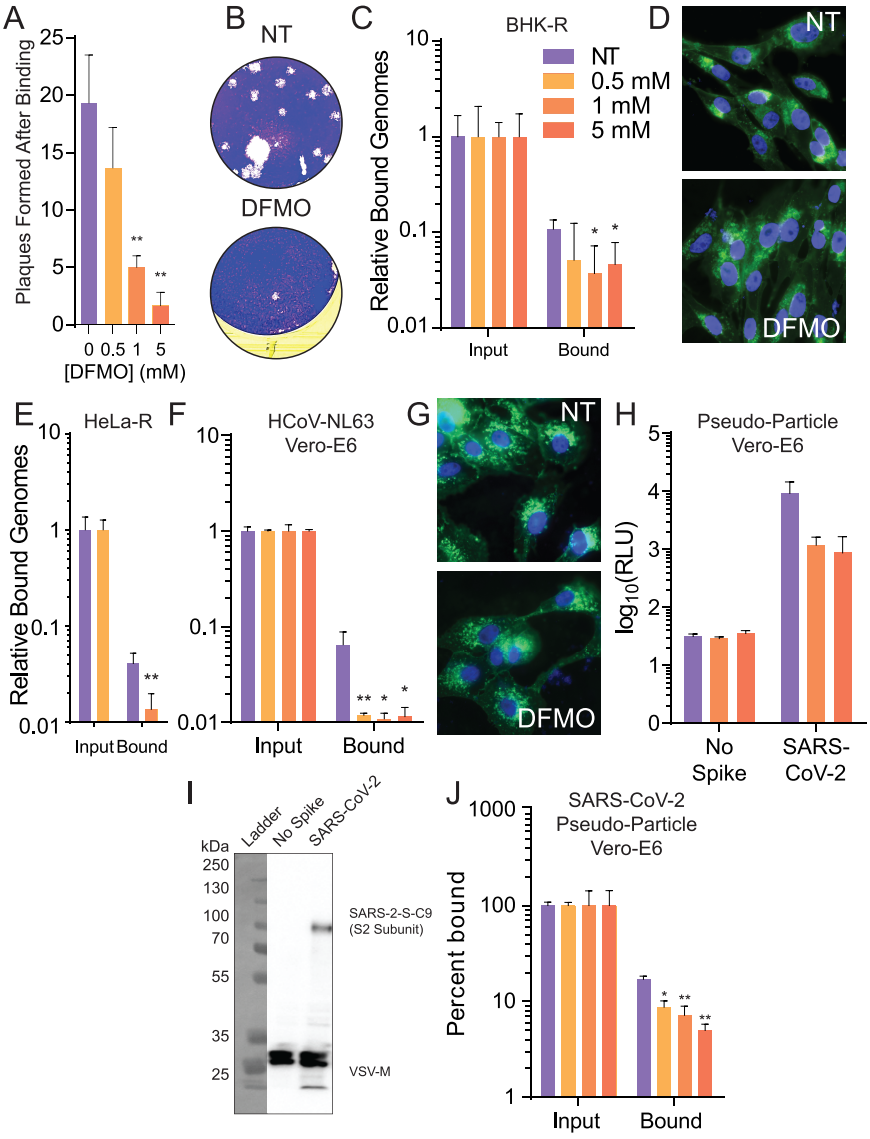

Figure 4. Polyamines facilitate coronavirus cellular attachment. Confluent BHK-R cells were treated with DFMO prior to the MHV binding assay. Virus was inoculated on cells for 5 min prior to removal, wash, and agarose overlay in media without DFMO. Plaques formed were quantified (A), and representative images from 1 mM DFMO treatment are shown (B). (C) BHK-R cells were treated as in (A), but after washing unattached virus, attached virus and cells were collected for RNA purification, reverse transcription, and viral genome quantitation by qPCR. Attached genomes were normalized to input virus. (D) MHV receptor (CECAM-1) was visualized on untreated and 1 mM DFMO treated cells. (E) HeLa-R cells were treated with 1 mM DFMO, infected with MHV, and processed as in (C). (F) Vero-E6 cells were treated with DFMO and analyzed for binding ability of HCoV-NL63 as in (C). (G) ACE2 expression on Vero-E6 cells was confirmed by immunofluorescence. (H) Pseudotyped viral particles with no viral glycoproteins or the SARS-CoV-2 spike were tested for their ability to bind and enter Vero-E6 cells. (I) Spike protein was confirmed to be present on pseudotyped virus by western blot. (J) Vero-E6 cells were treated with DFMO and infected with SARS-CoV-2 pseudoparticles as in (C). $*p < 0.05$, $**p < 0.01$, and $***p < 0.001$ by the Student's t test. Data from at least three independent experiments.

observed that the attachment was sensitive to DFMO treatment (Figure 4E). Again, we noted no change in viral receptor expression (ACE2, Figure 4G). Taking advantage of a pseudoparticle system as previously described[29] and adapted to SARS-CoV-2, we measured the attachment of SARS-CoV-2 to DFMO-treated cells. We verified that these pseudoparticles were competent to bind susceptible cells compared to "bald" particles, lacking viral spike (Figure 4H), and we confirmed the presence of the spike protein on purified particles by western blot (Figure 4I). We observed a reduction in cellular attachment of SARS-CoV-2 pseudoparticles in a dose-dependent manner (Figure 4H). Thus, human coronaviruses, including pandemic SARS-CoV-2, are sensitive to polyamine depletion and rely on polyamines for efficient cellular attachment.

Additional Molecules Targeting the Polyamine and Hypusination Pathway Quell Coronavirus Infection. Several pharmaceuticals target polyamine biosynthesis (Figure 5A) and exhibit antiviral activity,[16,19] though coronaviruses have not been thoroughly tested. Additionally, an offshoot of the polyamine pathway, the cellular hypusination pathway, in which spermidine is conjugated to eIF5A, plays roles in cellular translation,[30] which is critical for filovirus replication.[16,31] To determine if additional compounds targeting the polyamine and hypusination pathways exhibited activity against coronaviruses, we treated cells with increasing doses of inhibitors of

https://dx.doi.org/10.1021/acsinfecdis.0c00491
ACS Infect. Dis. XXXX, XXX, XXX−XXX

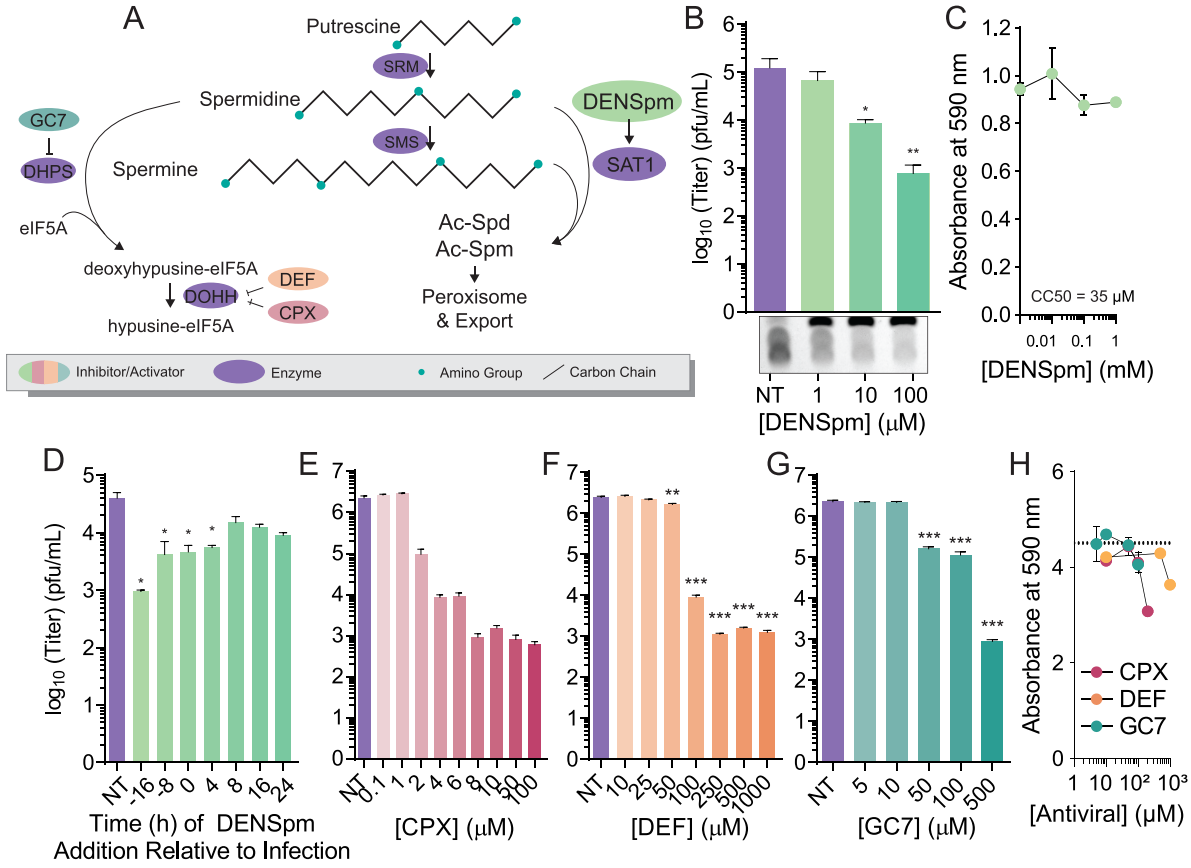

Figure 5. Additional molecules targeting the polyamine pathway quell coronavirus infection. (A) Schematic of the polyamine and hypusination pathway. (B) HeLa-R cells were treated with escalating doses of DENSpm for 16 h prior to infection with MHV at an MOI of 0.01. Viral titers were determined at 48 hpi (upper). Polyamine levels were measured by chromatography (lower). (C) Treated cells were assayed for viability after 16 h of treatment with DENSpm. (D) HeLa-R cells were treated with DENSpm at the indicated times before and after infection with MHV at an MOI of 10. Viral titers were determined at 48 hpi. BHK-R cells were treated with (E) CPX, (F) DEF, and (G) GC7 for 24 h prior to infection with MHV at an MOI of 0.01. Viral titers were determined at 48 hpi. (H) BHK-R cells treated with CPX, DEF, and GC7 were analyzed for cell viability after 24 h of treatment. *$p < 0.05$, **$p < 0.01$, and ***$p < 0.001$ by the Student's t test. Data from at least three independent experiments.

these pathways. We used the molecules diethylnorspermidine (DENSpm; enhances spermidine−spermine acetyltransferase [SAT1] activity and polyamine breakdown), GC7 (inhibits deoxyhypusine synthase [DHPS] to prevent eIF5A hypusination), and deferiprone and ciclopirox (DEF and CPX; inhibit deoxyhypusine hydroxylase [DOHH]) because they target distinct steps in the polyamine pathway. DENSpm significantly reduced polyamine levels and MHV titers at 10 μM (Figure 5B) with an IC50 of 1.6 μM. We observed minimal toxicity (Figure 5C) with a CC50 value of 35 μM resulting in a selectivity index of 23. Because DENSpm activates SAT1 to deplete polyamines, its action is much more rapid than DFMO. Thus, we tested whether DENSpm exhibited antiviral activity after the initiation of infection. Cells were treated with DENSpm at times before and after infection, and virus titers were measured at 48 hpi. We observed that DENSpm was most effective when treatment was initiated before infection; however, significant antiviral activity was maintained when DENSpm was added as late as 4 hpi (Figure 5D). Finally, we tested the hypusination inhibitors GC7, DEF, and CPX. We observed in all cases that these molecules significantly reduced MHV replication in a dose-dependent manner (Figure 5E−G) and that cytotoxicity was minimal (Figure 5H; summarized in Table 1). Thus, molecules targeting an additional branch of the polyamine biosynthetic pathway exhibit anti-coronavirus activity.

DISCUSSION

Polyamines are crucial to virus infection; however, their role in coronavirus replication was previously unknown. Here, we demonstrated that polyamines are essential to coronavirus infection and that attachment is at least one of the steps affected by polyamine depletion. We previously demonstrated that enteroviruses are similarly sensitive to polyamine depletion and rely on these polyamines for attachment.[15] This phenotype is conserved among several viral families, suggesting that polyamines may mediate a common attachment factor. Whether polyamines directly facilitate attachment by mediating virus−cell connections is unclear, and future work will be needed to delineate precisely how polyamines affect attachment. In addition to attachment, we observed that inhibitors of the hypusination pathway impact virus replication, suggesting that polyamines may facilitate infection through eIF5A hypusination, as observed for Ebolavirus.[16] Given the role of hypusinated eIF5A in translation, inhibitors of this pathway may directly inhibit viral translation or may inhibit the translation of a cellular factor essential to virus replication. Regardless, targeting polyamines may affect multiple steps of

https://dx.doi.org/10.1021/acsinfecdis.0c00491
ACS Infect. Dis. XXXX, XXX, XXX−XXX

infection, and additional work will be needed to uncover additional mechanisms.

Polyamines play several important roles in the cell, and recent work has highlighted pathways that may modulate virus replication. Spermidine, as a substrate for eIF5A hypusination, enhances cellular autophagy,[32] and recent work has suggested that spermidine-enhanced autophagy limits SARS-CoV-2 replication.[24] In contrast, our results suggest that spermidine does not inhibit or restrict virus replication at concentrations up to 100 μM. We do observe that spermine supplementation to cells reduces virus replication; however, we also observe significant cytotoxicity with spermine treatment, likely the reason for reduced titers. Additionally, we observed that DFMO treatment reduced polyamine content within cells, even at concentrations that did not affect viral titers. These data suggest that coronaviruses require a low concentration of polyamines for robust replication. In fact, bunyaviruses and alphaviruses replicate with supplementation of 100 nM polyamines in polyamine depleted cells.[14,33] Thus, these viruses may have evolved mechanisms to take advantage of polyamines even at low concentrations. This has implications for the molecular interactions between polyamines and coronaviruses, and perhaps coronaviruses evolved a strong affinity for polyamines. This also has implications for infection in an organism, as polyamines are transported between cells. In cancer therapies, polyamine transporter inhibitors can be used in conjunction with polyamine depletion agents to prevent both polyamine synthesis and internalization. While this has not been tested in the context of virus infection, the combination of inhibitors of synthesis and transport may more effectively reduce virus replication. Precisely how polyamines play into cellular signaling and metabolic pathways to affect virus replication is not clear; however, the complex interplay between metabolism and virus replication affords several opportunities to target virus replication with small molecule inhibitors.

With the current SARS-CoV-2 outbreak and the resulting coronavirus disease of 2019 (COVID-19), novel antivirals are urgently needed. Remdesivir has shown significant potential clinically,[34−37] and additional clinical testing will determine if this molecule can effectively treat infected individuals. Our work with DFMO and polyamine depletion highlights another promising intervention. An important limitation of our study is the relatively high concentration of drug required to reduce coronavirus infection. Given this caveat, the possibility of off-target antiviral effects cannot be ignored. However, we show that DFMO's antiviral effects are reversed by the addition of exogenous polyamines, suggesting specificity. Our prior results with chikungunya, Zika, Coxsackie, and Rift Valley fever viruses have demonstrated that low micromolar concentrations of inhibitor are sufficient to reduce virus replication. Thus, coronaviruses may be less reliant on polyamines than other viral families, though this requires significant further investigation.

Importantly, we observe that polyamine depletion functions prophylactically to reduce virus replication and may not reduce viral titers after the initiation of infection. Given the limits to our *in vitro* studies, we cannot say for certain whether polyamine depletion in a human could reduce virus replication or improve clinical outcome when treatment commences after exposure. However, polyamine depletion may be most effective as a prophylactic, preventing infection of vulnerable populations. With the significant spread of SARS-CoV-2, protecting vulnerable populations, including the elderly and immunocompromised, is essential to reducing mortality. Further, prophylactically treating frontline workers, including medical staff, could reduce the spread of the virus in a hospital setting. Currently, DFMO is approved for human use as a topical and intravenous agent. Nebulization and direct lung delivery, if effective at depleting polyamines in the lung, would be a benefit for reducing virus burden, but this remains untested. Whether DFMO or other polyamine-targeting drugs are sufficient to do this is unclear and requires significantly more investigation, including in animal models.

METHODS

Cell Culture. Cells were maintained in Dulbecco's modified Eagle's medium (DMEM; Life Technologies) with bovine serum and penicillin−streptomycin at 37 °C and 5% CO_2. Vero cells were obtained through BEI Resources, and VeroE6 cells were obtained through ATCC (CRL-1586). Vero and HeLa-R cells were supplemented with 10% new-born calf serum (NBCS; Thermo-Fischer). BHK-R cells were kindly provided by Dr. Susan Baker and were supplemented with 10% fetal bovine serum (FBS; Thermo-Fischer). HEK293T cells were grown in 10% FBS.

Infection and Enumeration of Viral Titers. MHV-A59 was derived from the first passage of virus in BHK-R cells from an infectious clone. SARS-CoV-2, isolate BetaCoV/France/IDF0372/2020 C2, was supplied by the National Reference Centre for Respiratory Viruses hosted at Institut Pasteur (Paris, France). The human sample from which this strain was isolated was provided by Dr. X. Lescure and Pr. Y. Yazdanpanah from the Bichat Hospital, Paris, France. Viral stocks were prepared by propagation in Vero E6 cells in DMEM supplemented with 2% FBS. All experiments involving live SARS-CoV-2 were performed in compliance with the Institut Pasteur guidelines for Biosafety Level 3 work. For all infections, DFMO was maintained throughout the infection as designated. Viral stocks were maintained at −80 °C. For infection, virus was diluted in serum-free DMEM for a multiplicity of infection (MOI) of 0.01 on BHK-R cells, unless otherwise indicated. Viral inoculum was added to the cells, and supernatants were collected at specified time points. To quantify viral titers via plaque assay, dilutions of cell supernatant were prepared in serum-free DMEM and used to inoculate confluent monolayers of BHK-R cells for 10 to 15 min at 37 °C. Cells were overlain with 0.8% agarose in DMEM containing 2% FBS. MHV-A59 samples were incubated for 2 days at 37 °C. Cells were fixed with 4% formalin and revealed with crystal violet solution (10% crystal violet; Sigma-Aldrich). Plaques were enumerated and used to back-calculate the number of plaque forming units (PFU) per milliliter of collected volume.

Drug Treatments. Difluoromethylornithine (DFMO; TargetMol) was diluted to a 100 mM solution in sterile PBS. For DFMO treatments, cells were trypsinized (Zymo Research) and reseeded with fresh medium supplemented with 2% FBS. Cells were treated with 1 mM DFMO unless otherwise indicated. Cells were incubated with DFMO for 96 h to allow for the depletion of polyamines. Experiments involving polyamine rescues were performed using 1 μM polyamines (Sigma-Aldrich) added to either the cell supernatant or viral inoculum as indicated.

Thin Layer Chromatography of Polyamines. Polyamines were separated by thin layer chromatography as

https://dx.doi.org/10.1021/acsinfecdis.0c00491
ACS Infect. Dis. XXXX, XXX, XXX−XXX

previously described.[38] For all samples, cells were treated as described prior to being trypsinized and centrifuged. Pellets were washed with PBS and then resuspended in 200 μL of 2% perchloric acid. Samples were then incubated overnight at 4 °C. Supernatant or 1 μmole of putrescine, spermidine, or spermine standards was combined with 5 mg/mL dansyl chloride (Sigma-Aldrich) in acetone and saturated sodium bicarbonate. Samples were incubated in the dark overnight at room temperature. Excess dansyl chloride was cleared by incubating the reaction with proline (Sigma-Aldrich). Dansylated polyamines were extracted with toluene (Sigma-Aldrich) and centrifuged. The sample was added in spots to the silica gel matrix TLC plates (Sigma-Aldrich) and exposed to ascending chromatography with 1:1 cyclohexane/ethyl acetate. The plate was dried and visualized via exposure to UV.

Plaque Formation Attachment Assay. BHK-R cells were seeded in 6-well plates and grown to confluence in DMEM with 2% FBS. The cells were treated for 96 h with varying concentrations of DFMO. After the 96 h DFMO treatment, the media were aspirated from the cells and replaced with 500 μL of serum free media containing 1000 PFU MHV. The infected cells were incubated at room temperature or on ice for 5 min. Cells were washed 3× with PBS and then overlaid with 0.8% agarose containing DMEM with 2% FBS. The plates were incubated at 37 °C for 2 days for plaques to develop. The cells were fixed with 4% formalin, and the plaques were visualized with crystal violet staining.

Plaque Size Measurement. BHK-R or HeLa-R cells were seeded in 6-well plates and grown to confluence. Approximately 100 PFU of MHV-A59 was diluted in a 500 μL inoculum of serum free DMEM. The inoculum was incubated on the cells for approximately 30 min at 37 °C. After 30 min, an overlay of 8 mL of 0.8% agarose containing DMEM with 2% FBS (BHK-R) or NBCS (HeLa-R) was added to each well. The dishes were incubated at 37 °C for 2 days to allow plaque formation. The cells were fixed with 4% formalin, and the agarose plugs were removed. The fixed cells were stained with crystal violet. Plaque size was determined using ImageJ software.[39]

Immunofluorescence Imaging. Cells grown on coverslips were either treated with 1 mM DFMO or untreated. Cells were fixed with 4% formalin for 15 min, washed with PBS, permeabilized, and blocked with 0.2% Triton X-100 and 2% BSA in PBS (blocking solution) for 30 min at room temperature (RT). Cells were sequentially incubated as follows: primary rabbit anti-hACE2 (Invitrogen, SN0754) (Vero E6) or rabbit anti-mCEACAM (BHK-R) antibodies (1:500) with blocking for 2 h at room temperature. Cells were subsequently washed then incubated with secondary goat anti-rabbit antibodies (1:500 with blocking, 30 min, RT). Mounting media with DAPI was used to visualize nuclei. Samples were imaged with a Zeiss Axio Observer 7 with Lumencor Spectra X LED light system and a Hamamatsu Flash 4 camera using appropriate filters using Zen Blue software with a 40× objective.

Western Blot. Samples were collected with Bolt LDS Buffer and Bolt Reducing Agent (Invitrogen) and run on polyacrylamide gels. Gels were transferred using the iBlot 2 Gel Transfer Device (Invitrogen). Membranes were probed with primary antibodies for mouse anti-rhodopsin (EMD Millipore, MAB5356), anti-VSV-M (23H12), and anti-mouse IgG (Goat, HRP-Labeled, NEF822001EA). Membranes were treated with SuperSignal West Pico PLUS Chemiluminescent Substrate (ThermoFisher Scientific) and visualized on a ProteinSimple FluorChem E imager.

RNA Purification and cDNA Synthesis. Media were cleared from cells, and Trizol reagent (Zymo Research) was added directly. Lysate was then collected, and RNA was purified through a Zymo RNA extraction kit. Purified RNA was subsequently used for cDNA synthesis using High Capacity cDNA Reverse Transcription Kits (Thermo-Fischer), according to the manufacturer's protocol, with 10−100 ng of RNA and random hexamer primers.

qPCR-Based Attachment Assay. BHK-R, HeLa-R, and Vero cells were seeded at 4×10^4 cells per well in 24-well plates in DMEM with either 2% FBS or NBCS. The cells were treated for 96 h with varying concentrations of DFMO. After 96 h, the media were aspirated from the cells and replaced with 100 μL of serum free media containing virus. The infected cells were incubated for 5 min at room temperature or on ice. The cells were then washed 1× with PBS, and then, 200 μL of Trizol was added to the cells. The RNA was extracted with the Zymo RNA extraction kit, converted to cDNA, and quantified by real-time PCR with SYBR Green (DotScientific) using the one-step protocol QuantStudio 3 (ThermoFisher Scientific). Relative genomes were calculated using the ΔC^T method, normalized to the β-actin qRT-PCR control, and calculated as the fraction of the unwashed samples. Primer sequences are as follows: NL63, 5′-TGT-CAA-CGA-GGT-TTT-GCA-TTA-AAT-3′ (F) and 5′-ACT-GGC-CTA-CCA-TTG-TGT-GTA-AGA-3′ (R); MHV, 5′-ATC-CTC-AAG-AAG-ACC-ACT-TGG-GCT-GAC-3′ (F) and 5′-GAG-TAA-TGG-GGA-ACC-ACA-CTC−CCG-3′ (R); β-actin, 5′-CAC-TCT-TCC-AGC-CTT-CCT-TC-3′ (F) and 5′-GTA-CAG-GTC-TTT-GCG-GAT-GT-3′ (R). Primers were verified for linearity using 8-fold serial diluted cDNA and checked for specificity via melt curve analysis. SARS-CoV-2 genomes were detected using a Taqman assay (IP4 set) as described on the WHO Web site (https://www.who.int/docs/default-source/coronaviruse/real-time-rt-pcr-assays-for-the-detection-of-sars-cov-2-institut-pasteur-paris.pdf?sfvrsn=3662fcb6_2)

Synthesis of SARS-CoV-2 Pseudovirus. 293T cells were seeded into a 150 mm tissue culture dish 24 h prior to transfection. Cells were transfected with a SARS-CoV-2 spike using LipoD293 and following the manufacture's protocol. After 6 h, the media were removed and replaced with fresh, prewarmed 10% FBS media. The following day, cells were infected with a 1 to 100 dilution of Fluc-VSV-Junin virus and allowed to infect for 2 h. After the 2 h, the cells were washed 2× with serum free DMEM, and fresh, prewarmed media were placed onto the cells. On the following day, cell supernatant was collected and spun down via differential centrifugation (300*g* for 10 min at 4 °C, 4500*g* for 10 min at 4 °C) and stored at −80 °C.

Pseudovirus Attachment Assay. Vero E6 cells were seeded at 4×10^4 in 24-well plates in DMEM with 2% NBCS. Cells were then treated with varying concentrations of DFMO for 96 h. After 96 h, the media were aspirated from the cells and replaced with 100 μL of serum free media containing pseudovirus. The infected cells were incubated for 5 min at room temperature. Pseudovirus was then aspirated off and washed 1× with PBS (bound), and new, prewarmed 2% NBCS media were added to the cells and allowed to sit overnight (input and bound). The following day, the media were aspirated from the cells, and the cells were then washed with 1× PBS. Subsequently, cells were then lysed with 75 μL of 1×

https://dx.doi.org/10.1021/acsinfecdis.0c00491
ACS Infect. Dis. XXXX, XXX, XXX−XXX

Pierce Lysis Buffer (Promega) for 10 min. The lysed samples were then transferred to a white, opaque 96-well plate. 150 μL of luciferase was added to wells and read with a GlowMax luminometer. The percent bound was calculated by normalizing luciferase values to the input.

Genome/PFU Ratio. Cells were infected with the MHV-A59 at an MOI of 0.01. Supernatant was collected 48 hpi. The infectious virus (PFU) was quantified via plaque assay as described. RNA was extracted, reverse-transcribed, and quantified with qPCR as described above.

Statistical Analysis. Prism 6 (GraphPad) was used to generate graphs and perform statistical analysis. For all analyses, the two-tailed Student's t test was used to compare groups, unless otherwise noted, with $a = 0.05$. For tests of sample proportions, p values were derived from the calculated Z scores with two tails and $a = 0.05$.

AUTHOR INFORMATION

Corresponding Author

Bryan C. Mounce − *Department of Microbiology and Immunology, Stritch School of Medicine, Loyola University Chicago, Maywood, Illinois 60153, United States;* orcid.org/0000-0003-1710-5362; Phone: 708 216 3358; Email: bmounce@luc.edu

Authors

Mason R. Firpo − *Department of Microbiology and Immunology, Stritch School of Medicine, Loyola University Chicago, Maywood, Illinois 60153, United States*

Vincent Mastrodomenico − *Department of Microbiology and Immunology, Stritch School of Medicine, Loyola University Chicago, Maywood, Illinois 60153, United States*

Grant M. Hawkins − *Department of Microbiology and Immunology, Stritch School of Medicine, Loyola University Chicago, Maywood, Illinois 60153, United States*

Matthieu Prot − *G5 Evolutionary Genomics of RNA Viruses, Institut Pasteur, Paris 75015, France*

Laura Levillayer − *Functional Genetics of Infectious Diseases Unit, Institut Pasteur, Paris 75015, France*

Tom Gallagher − *Department of Microbiology and Immunology, Stritch School of Medicine, Loyola University Chicago, Maywood, Illinois 60153, United States;* orcid.org/0000-0002-8601-5961

Etienne Simon-Loriere − *G5 Evolutionary Genomics of RNA Viruses, Institut Pasteur, Paris 75015, France*

Complete contact information is available at: https://pubs.acs.org/10.1021/acsinfecdis.0c00491

Notes

The authors declare no competing financial interest.

ACKNOWLEDGMENTS

We thank Susan Baker for generous assistance with the MHV system and for providing the virus and cells as well as Ivana Kuo for microscopy assistance. We also thank Susan Uprichard for critical discussion of the data. E.S.-L. acknowledges funding from the INCEPTION program (Investissements d'Avenir grant ANR-16-CONV-0005), from the Institut Pasteur corona task force, and from the Laboratoire d'Excellence "Integrative Biology of Emerging Infectious Diseases" (grant no. ANR-10-LABX-62-IBEID).

REFERENCES

(1) de Wit, E., van Doremalen, N., Falzarano, D., and Munster, V. J. (2016) SARS and MERS: Recent Insights into Emerging Coronaviruses. *Nat. Rev. Microbiol. 14* (8), 523−534.

(2) Gralinski, L. E., and Menachery, V. D. (2020) Return of the Coronavirus: 2019-NCoV. *Viruses 12* (2), 135.

(3) WHO (accessed 2020-06-06) *Middle East respiratory syndrome coronavirus (MERS-CoV)*, http://www.who.int/emergencies/mers-cov/en/.

(4) Pyrc, K., Dijkman, R., Deng, L., Jebbink, M. F., Ross, H. A., Berkhout, B., and van der Hoek, L. (2006) Mosaic Structure of Human Coronavirus NL63, One Thousand Years of Evolution. *J. Mol. Biol. 364* (5), 964−973.

(5) van der Hoek, L., Ihorst, G., Sure, K., Vabret, A., Dijkman, R., de Vries, M., Forster, J., Berkhout, B., and Uberla, K. (2010) Burden of Disease Due to Human Coronavirus NL63 Infections and Periodicity of Infection. *J. Clin. Virol. 48* (2), 104−108.

(6) Brown, A. J., Won, J. J., Graham, R. L., Dinnon, K. H., Sims, A. C., Feng, J. Y., Cihlar, T., Denison, M. R., Baric, R. S., and Sheahan, T. P. (2019) Broad Spectrum Antiviral Remdesivir Inhibits Human Endemic and Zoonotic Deltacoronaviruses with a Highly Divergent RNA Dependent RNA Polymerase. *Antiviral Res. 169*, 104541.

(7) Sheahan, T. P., Sims, A. C., Graham, R. L., Menachery, V. D., Gralinski, L. E., Case, J. B., Leist, S. R., Pyrc, K., Feng, J. Y., Trantcheva, I., Bannister, R., Park, Y., Babusis, D., Clarke, M. O., Mackman, R. L., Spahn, J. E., Palmiotti, C. A., Siegel, D., Ray, A. S., Cihlar, T., Jordan, R., Denison, M. R., and Baric, R. S. (2017) Broad-Spectrum Antiviral GS-5734 Inhibits Both Epidemic and Zoonotic Coronaviruses. *Sci. Transl. Med. 9* (396), eaal3653.

(8) Gerner, E. W., and Meyskens, F. L. (2004) Polyamines and Cancer: Old Molecules, New Understanding. *Nat. Rev. Cancer 4* (10), 781−792.

(9) Frugier, M., Florentz, C., Hosseini, M. W., Lehn, J. M., and Giegé, R. (1994) Synthetic Polyamines Stimulate in Vitro Transcription by T7 RNA Polymerase. *Nucleic Acids Res. 22* (14), 2784−2790.

(10) Mandal, S., Mandal, A., Johansson, H. E., Orjalo, A. V., and Park, M. H. (2013) Depletion of Cellular Polyamines, Spermidine and Spermine, Causes a Total Arrest in Translation and Growth in Mammalian Cells. *Proc. Natl. Acad. Sci. U. S. A. 110* (6), 2169−2174.

(11) Burri, C., and Brun, R. (2003) Eflornithine for the Treatment of Human African Trypanosomiasis. *Parasitol. Res. 90* (S1), S49−52.

(12) Milord, F., Pépin, J., Loko, L., Ethier, L., and Mpia, B. (1992) Efficacy and Toxicity of Eflornithine for Treatment of Trypanosoma Brucei Gambiense Sleeping Sickness. *Lancet 340* (8820), 652−655.

(13) Shapiro, J., and Lui, H. (2001) Vaniqa - Eflornithine 13.9% Cream. *Skin Therapy Letter 6* (7), 1.

(14) Mounce, B. C., Poirier, E. Z., Passoni, G., Simon-Loriere, E., Cesaro, T., Prot, M., Stapleford, K. A., Moratorio, G., Sakuntabhai, A., Levraud, J.-P., and Vignuzzi, M. (2016) Interferon-Induced Spermidine-Spermine Acetyltransferase and Polyamine Depletion Restrict Zika and Chikungunya Viruses. *Cell Host Microbe 20* (2), 167−177.

(15) Kicmal, T. M., Tate, P. M., Dial, C. N., Esin, J. J., and Mounce, B. C. (2019) Polyamine Depletion Abrogates Enterovirus Cellular Attachment. *J. Virol. 93*, e01054-19.

(16) Olsen, M. E., Filone, C. M., Rozelle, D., Mire, C. E., Agans, K. N., Hensley, L., and Connor, J. H. (2016) Polyamines and Hypusination Are Required for Ebolavirus Gene Expression and Replication. *mBio 7* (4), e00882-16.

(17) Mounce, B. C., Olsen, M. E., Vignuzzi, M., and Connor, J. H. (2017) Polyamines and Their Role in Virus Infection. *Microbiol. Mol. Biol. Rev. 81* (4), e00029-17.

(18) Firpo, M. R., and Mounce, B. C. (2020) Diverse Functions of Polyamines in Virus Infection. *Biomolecules 10* (4), 628.

(19) Mounce, B. C., Cesaro, T., Moratorio, G., Hooikaas, P. J., Yakovleva, A., Werneke, S. W., Smith, E. C., Poirier, E. Z., Simon-Loriere, E., Prot, M., Tamietti, C., Vitry, S., Volle, R., Khou, C., Frenkiel, M.-P., Sakuntabhai, A., Delpeyroux, F., Pardigon, N.,

https://dx.doi.org/10.1021/acsinfecdis.0c00491
ACS Infect. Dis. XXXX, XXX, XXX−XXX

Flamand, M., Barba-Spaeth, G., Lafon, M., Denison, M. R., Albert, M. L., and Vignuzzi, M. (2016) Inhibition of Polyamine Biosynthesis Is a Broad-Spectrum Strategy against RNA Viruses. *J. Virol. 90* (21), 9683−9692.

(20) Compton, S. R., Barthold, S. W., and Smith, A. L. (1993) The Cellular and Molecular Pathogenesis of Coronaviruses. *Lab. Anim. Sci. 43* (1), 15−28.

(21) Weiss, S. R., and Leibowitz, J. L. Coronavirus Pathogenesis. In *Advances in Virus Research*; Maramorosch, K., Shatkin, A. J., and Murphy, F. A., Eds.; Academic Press, 2011; Vol. *81*, Chapter 4, pp 85−164; DOI: 10.1016/B978-0-12-385885-6.00009-2.

(22) Leibowitz, J., Kaufman, G., and Liu, P. (2011) Coronaviruses: Propagation, Quantification, Storage, and Construction of Recombinant Mouse Hepatitis Virus. *Curr. Protoc. Microbiol. 21*, 15E.1.1−15E.1.46.

(23) Mastrodomenico, V., Esin, J. J., Graham, M. L., Tate, P. M., Hawkins, G. M., Sandler, Z. J., Rademacher, D. J., Kicmal, T. M., Dial, C. N., and Mounce, B. C. (2019) Polyamine Depletion Inhibits Bunyavirus Infection via Generation of Noninfectious Interfering Virions. *J. Virol. 93*, e00530-19.

(24) Gassen, N. C., Papies, J., Bajaj, T., Dethloff, F., Emanuel, J., Weckmann, K., Heinz, D. E., Heinemann, N., Lennarz, M., Richter, A., Niemeyer, D., Corman, V. M., Giavalisco, P., Drosten, C., and Müller, M. A. (2020) Analysis of SARS-CoV-2-Controlled Autophagy Reveals Spermidine, MK-2206, and Niclosamide as Putative Antiviral Therapeutics. *bioRxiv*, 2020.04.15.997254, DOI: 10.1101/2020.04.15.997254.

(25) Igarashi, K., and Kashiwagi, K. (2000) Polyamines: Mysterious Modulators of Cellular Functions. *Biochem. Biophys. Res. Commun. 271* (3), 559−564.

(26) Igarashi, K., and Kashiwagi, K. (2019) The Functional Role of Polyamines in Eukaryotic Cells. *Int. J. Biochem. Cell Biol. 107*, 104−115.

(27) Mastrodomenico, V., Esin, J. J., Qazi, S., Omoba, O. S., Fung, B. L., Khomutov, M. A., Ivanov, A. V., Mukhopadhyay, S., and Mounce, B. C. (2020) Virion-Associated Spermidine Transmits with Rift Valley Fever Virus Particles to Maintain Infectivity. *bioRxiv*, 2020.01.23.915900, DOI: 10.1101/2020.01.23.915900.

(28) Wolf, J. E., Shander, D., Huber, F., Jackson, J., Lin, C.-S., Mathes, B. M., and Schrode, K. (2007) Eflornithine HCl Study Group. Randomized, Double-Blind Clinical Evaluation of the Efficacy and Safety of Topical Eflornithine HCl 13.9% Cream in the Treatment of Women with Facial Hair. *Int. J. Dermatol. 46* (1), 94−98.

(29) Qing, E., Hantak, M., Perlman, S., and Gallagher, T. (2020) Distinct Roles for Sialoside and Protein Receptors in Coronavirus Infection. *mBio 11* (1), No. e02764-19.

(30) Park, M. H., and Wolff, E. C. (2018) Hypusine, a Polyamine-Derived Amino Acid Critical for Eukaryotic Translation. *J. Biol. Chem. 293* (48), 18710−18718.

(31) Olsen, M. E., Cressey, T. N., Mühlberger, E., and Connor, J. H. (2018) Differential Mechanisms for the Involvement of Polyamines and Hypusinated EIF5A in Ebola Virus Gene Expression. *J. Virol. 92*, e01260-18.

(32) Zhang, H., Alsaleh, G., Feltham, J., Sun, Y., Napolitano, G., Riffelmacher, T., Charles, P., Frau, L., Hublitz, P., Yu, Z., Mohammed, S., Ballabio, A., Balabanov, S., Mellor, J., and Simon, A. K. (2019) Polyamines Control EIF5A Hypusination, TFEB Translation, and Autophagy to Reverse B Cell Senescence. *Mol. Cell 76* (1), 110−125.E9.

(33) Mastrodomenico, V., Esin, J. J., Qazi, S., Khomutov, M. A., Ivanov, A. V., Mukhopadhyay, S., and Mounce, B. C. (2020) Virion-Associated Polyamines Transmit with Bunyaviruses to Maintain Infectivity and Promote Entry. *ACS Infect. Dis. 6* (9), 2490−2501.

(34) Beigel, J. H., Tomashek, K. M., Dodd, L. E., Mehta, A. K., Zingman, B. S., Kalil, A. C., Hohmann, E., Chu, H. Y., Luetkemeyer, A., Kline, S., Lopez de Castilla, D., Finberg, R. W., Dierberg, K., Tapson, V., Hsieh, L., Patterson, T. F., Paredes, R., Sweeney, D. A., Short, W. R., Touloumi, G., Lye, D. C., Ohmagari, N., Oh, M.-D., Ruiz-Palacios, G. M., Benfield, T., Fätkenheuer, G., Kortepeter, M. G., Atmar, R. L., Creech, C. B., Lundgren, J., Babiker, A. G., Pett, S., Neaton, J. D., Burgess, T. H., Bonnett, T., Green, M., Makowski, M., Osinusi, A., Nayak, S., and Lane, H. C. (2020) ACTT-1 Study Group Members. Remdesivir for the Treatment of Covid-19 - Preliminary Report. *N. Engl. J. Med.*, DOI: 10.1056/NEJMoa2007764.

(35) Goldman, J. D., Lye, D. C. B., Hui, D. S., Marks, K. M., Bruno, R., Montejano, R., Spinner, C. D., Galli, M., Ahn, M.-Y., Nahass, R. G., Chen, Y.-S., SenGupta, D., Hyland, R. H., Osinusi, A. O., Cao, H., Blair, C., Wei, X., Gaggar, A., Brainard, D. M., Towner, W. J., Muñoz, J., Mullane, K. M., Marty, F. M., Tashima, K. T., Diaz, G., and Subramanian, A. (2020) GS-US-540−5773 Investigators. Remdesivir for 5 or 10 Days in Patients with Severe Covid-19. *N. Engl. J. Med.*, DOI: 10.1056/NEJMoa2015301.

(36) Grein, J., Ohmagari, N., Shin, D., Diaz, G., Asperges, E., Castagna, A., Feldt, T., Green, G., Green, M. L., Lescure, F.-X., Nicastri, E., Oda, R., Yo, K., Quiros-Roldan, E., Studemeister, A., Redinski, J., Ahmed, S., Bernett, J., Chelliah, D., Chen, D., Chihara, S., Cohen, S. H., Cunningham, J., D'Arminio Monforte, A., Ismail, S., Kato, H., Lapadula, G., L'Her, E., Maeno, T., Majumder, S., Massari, M., Mora-Rillo, M., Mutoh, Y., Nguyen, D., Verweij, E., Zoufaly, A., Osinusi, A. O., DeZure, A., Zhao, Y., Zhong, L., Chokkalingam, A., Elboudwarej, E., Telep, L., Timbs, L., Henne, I., Sellers, S., Cao, H., Tan, S. K., Winterbourne, L., Desai, P., Mera, R., Gaggar, A., Myers, R. P., Brainard, D. M., Childs, R., and Flanigan, T. (2020) Compassionate Use of Remdesivir for Patients with Severe Covid-19. *N. Engl. J. Med. 382*, 2327.

(37) Wang, Y., Zhang, D., Du, G., Du, R., Zhao, J., Jin, Y., Fu, S., Gao, L., Cheng, Z., Lu, Q., Hu, Y., Luo, G., Wang, K., Lu, Y., Li, H., Wang, S., Ruan, S., Yang, C., Mei, C., Wang, Y., Ding, D., Wu, F., Tang, X., Ye, X., Ye, Y., Liu, B., Yang, J., Yin, W., Wang, A., Fan, G., Zhou, F., Liu, Z., Gu, X., Xu, J., Shang, L., Zhang, Y., Cao, L., Guo, T., Wan, Y., Qin, H., Jiang, Y., Jaki, T., Hayden, F. G., Horby, P. W., Cao, B., and Wang, C. (2020) Remdesivir in Adults with Severe COVID-19: A Randomised, Double-Blind, Placebo-Controlled, Multicentre Trial. *Lancet 395* (10236), 1569−1578.

(38) Madhubala, R. (1997) Thin-Layer Chromatographic Method for Assaying Polyamines. *Methods Mol. Biol. 79*, 131−136.

(39) Schneider, C. A., Rasband, W. S., and Eliceiri, K. W. (2012) NIH Image to ImageJ: 25 Years of Image Analysis. *Nat. Methods 9* (7), 671−675.

https://dx.doi.org/10.1021/acsinfecdis.0c00491
ACS Infect. Dis. XXXX, XXX, XXX−XXX